Translational Stroke Research
https://doi.org/10.1007/s12975-024-01261-w

REVIEW

Imaging of Intracranial Aneurysms: A Review of Standard and Advanced Imaging Techniques

Sricharan S. Veeturi[1,2] · Samuel Hall[3] · Soichiro Fujimura[4,5] · Mahmud Mossa-Basha[6] · Elena Sagues[7] · Edgar A. Samaniego[7] · Vincent M. Tutino[1,8]

Received: 16 April 2024 / Revised: 16 April 2024 / Accepted: 13 May 2024

Abstract

The treatment of intracranial aneurysms is dictated by its risk of rupture in the future. Several clinical and radiological risk factors for aneurysm rupture have been described and incorporated into prediction models. Despite the recent technological advancements in aneurysm imaging, linear length and visible irregularity with a bleb are the only radiological measure used in clinical prediction models. The purpose of this article is to summarize both the standard imaging techniques, including their limitations, and the advanced techniques being used experimentally to image aneurysms. It is expected that as our understanding of advanced techniques improves, and their ability to predict clinical events is demonstrated, they become an increasingly routine part of aneurysm assessment. It is important that neurovascular specialists understand the spectrum of imaging techniques available.

Keywords Unruptured intra-cranial aneurysm · Rupture risk · Angiography · Vessel wall imaging

Introduction

Unruptured intracranial aneurysms (UIA) are cerebral outpouchings that can rupture and cause subarachnoid hemorrhage (SAH) which has a high mortality and morbidity rate. A meta-analysis by Vlak et al. estimated the prevalence of UIA to be 3.2% in adults 50 years old [1]. Populations with certain comorbidities including autosomal dominant polycystic kidney disease (ADPKD) (prevalence ratio = 6.9), family history of intracranial aneurysms (prevalence ratio = 3.4), and female gender (prevalence ratio = 2.2) [1]. Among populations of particular conditions, the prevalence of aneurysms is particularly high such as Marfan syndrome (12%) [2] and ADPKD (9%) [3]. UIA may also be more prevalent in older adults [4, 5]. The aneurysms identified in these population studies are most likely to be < 7 mm [1, 4] and found in the anterior circulation although it is inconsistent which is the most common location between middle cerebral artery (MCA) [1], anterior communicating artery (AComm) [6], or internal carotid artery (ICA) [4]. Prevalence of UIAs also varies based on the geographic population as indicated in a population-based study by Greving et al. Herein, the authors found that individuals of Japanese and Finnish origin had a 2.8 and 3.6 times increased risk of IA rupture, respectively.

Sricharan S. Veeturi and Samuel Hall contributed equally.

✉ Vincent M. Tutino
vincentt@buffalo.edu

1 Canon Stroke and Vascular Research Center, Clinical and Translational Research Center, University at Buffalo, 875 Ellicott Street, Buffalo, NY 14214, USA

2 Department of Neurosurgery, University at Buffalo, Buffalo, NY, USA

3 Department of Neurosurgery, University Hospital Southampton NHS Foundation Trust, Southampton, UK

4 Department of Mechanical Engineering, Tokyo University of Science, Tokyo, Japan

5 Division of Innovation for Medical Information Technology, The Jikei University School of Medicine, Tokyo, Japan

6 Department of Radiology, University of Washington, Seattle, USA

7 Department of Neurology, University of Iowa, Iowa City, IA, USA

8 Department of Pathology and Anatomical Sciences, University at Buffalo, Buffalo, NY, USA

Published online: 10 June 2024

Imaging of IAs is paramount for management of UIAs. The first ever use of angiography for visualization of cerebral vessels was in 1927 by Egas Moniz [7, 8]. Moniz named this procedure "arterial encephalography" as the theory of it was to improve contrast of blood vessels by injecting opaque material in the blood vessels not unlike the then common practice of using pseudo-encephalography developed by Dandy[9]. Since then, imaging techniques have evolved concurrently with our knowledge of IA natural history. From the routine clinical imaging which enables clinicians to identify potential IAs without autopsy, to risk assessment and successive treatment planning, imaging is needed for the entire IA management pipeline. Indeed, imaging plays a key role in determining IA size and morphology which forms the basis of clinical risk stratification of IAs. Lastly, imaging is crucial to the treatment of IAs, namely during endovascular treatment which is done using fluoroscopic imaging such as digital subtraction angiography which will be discussed in subsequent sections.

The purpose of this review is to understand the role of imaging in detection and clinical management of IAs and to reflect on standard as well as non-traditional imaging of IAs. For standard imaging, the purpose, advantages, and limitations of computed tomography angiography (CTA), magnetic resonance angiography (MRA), and digital subtraction angiography (DSA) are discussed in subsequent sections. Additionally, we will also discuss other emerging advanced imaging modalities, namely vessel wall imaging (VWI), 4D flow, and 4D CTA. Finally, we will review the potential usage of artificial intelligence (AI) in routine clinical imaging. AI can be used to enhance existing imaging, better risk stratification, and treatment planning as will be discussed in upcoming sections.

Role of Imaging in Risk Assessment of *IA*

Clinical imaging provides precise visualization of intracranial vessels and hence, can assist in better and early detection of IAs. Clinical risk assessment of IAs is primary based on size and morphology of the IA at the time of imaging with large and irregular IAs being at higher risk of rupture than smaller more regular ones [10]. Imaging enables robust 3D quantification of IA size and morphology thus helping in robust risk stratification [11]. Furthermore, morphology of IA has also been associated with long-term treatment outcome [12]. Studies have shown that morphology of the IA at the time of imaging can help predict long-term outcome in patients treated with flow diverters as well as coils [13, 14].

Intersection of imaging and IA risk assessment happens in quantification of aneurysm size and morphology. The standard approaches to measuring aneurysm morphology include linear measurements and descriptions of sac shape. The simplest linear measurement, sac width in the longest dimension referred to as the IA size, is repeatedly borne out as a risk factor for rupture [15–17]. One of the first large cohort international studies aimed at using patient history and IA size for risk stratification was the ISUIA study [18]. Herein, the authors found that patients with previous SAH having IAs > 7 mm and located in either the internal carotid artery (ICA), middle cerebral artery (MCA), the anterior communicating artery (AComm), or especially the posterior communicating artery (PComm) had the highest risk of IA rupture over a 5-year period. They found that IA size had a relative risk of 3.3 for 7–12 mm IAs and 17.0 for IAs > 12 mm. Similarly, IA location had a relative risk of 2.1 for PComm, 0.15 for cavernous artery, and 2.3 for basilar tip IAs. In the PHASES Study, compared to < 5 mm, the rupture hazard ratio for size increases to 1.1, 2.4, 5.7, and 21.3 for aneurysms 5–7 mm, 7–10 mm, 10–20 mm, and > 20 mm, respectively [19]. Other linear measurements such as dome-neck ratio or aspect ratio have been examined in case–control studies, but none were included for primary analysis of the prospective natural history studies. A recent comprehensive meta-analysis, incorporating data from 13,025 aneurysms found that ruptured aneurysms typically presented with a size of 6.1 mm (95% CI, 5.6 to 6.5 mm). In contrast, unruptured aneurysms had a smaller average size of 4.9 mm (95% CI, 4.5 to 5.3 mm) [10]. Additionally, an aspect ratio of 1.5 (95% CI of 1.4 to 1.6) was identified as a marker for aneurysms that were ruptured at the time of presentation. This is compared to a lower aspect ratio of 1.1 (95% CI of 1.1 to 1.2), for aneurysms that had not ruptured.

In addition to size, IA morphology and irregularity also play a key role in risk assessment of IAs. The UCAS study [15], the largest contributor to PHASES, and the more recent prospective series by Murayama et al. [20] both identified the presence of a daughter sac as an indicator of high-risk IAs with a hazard ratio of 1.6 and 11.1, respectively. A subsequent case–control analysis of the ISUIA data found that neither a daughter nor multilobes were significantly associated with rupture; however, only a small number of cases of each were identified [21]. This study also looked at linear measurements and found that size-ratio and perpendicular height were significantly associated with ruptured aneurysms [21]. Accordingly, aneurysm shape is included in the ELAPPS score for predicting growth [22] and the UIATS consensus-based model for guiding treatment [23].

The increasing use of cranial imaging over recent decades is resulting in a higher number of incidental UIAs being diagnosed [24]. Less common routes to diagnosis include screening scans such as those with a positive family history or unruptured aneurysms presenting with symptoms such as the acute oculomotor nerve palsy, sentinel headache, vision loss, or embolic event [25]. Once the diagnosis is established, the risk assessment for rupture begins, starting with

standard imaging and progressing to newer advanced techniques. Standard imaging techniques such as CTA, MRA, and DSA can provide measurements of the aneurysm lumen and are the basis for the natural history data so far. Advanced techniques, including mural wall imaging such as vessel wall imaging (VWI), have not been prospectively assessed for their role in predicting rupture risk and incorporating them in UIA assessment varies between units. A recent ASNR survey of VWI use, predominantly from USA responders, found that only half of physicians are using VWI and only 40% of those are using for aneurysm assessment [26]. This is even lower in the UK where only 10% of units are using VWI for UIA assessment [27].

Standard Imaging Approaches

CTA

CTA is a cross-sectional imaging modality utilizing helical tomography. It is non-invasive and fast to acquire however has the disadvantages of requiring ionizing radiation and iodine-based contrast agents. Modern CT is developed to use multidetector arrays which are either 64, 128 or 256 rows and provide sub-millimeter resolution. Ultra-high-resolution CT can improve on this further with a resolution of 0.23mm and better artifact reduction techniques [28]. Recently, dual-energy computed tomography has also been introduced into the clinical setting which boasts a better tissue characterization as it involves using multiple X-ray spectra for. However, it is currently only used in <10% of clinics for head imaging purposes as a recent survey found out, primarily due to lack of experience [29].

The sensitivity of CT angiography for detecting aneurysms is referenced against DSA as the gold standard. Meta-analysis of CT angiography for detecting aneurysms identified an overall sensitivity of 97%, ranging from 93 to 99.2% when using single detector or 64-row multidetector scanners, respectively [30]. The number of detector rows has a more significant influence on smaller aneurysms. Single-detector arrays show similar sensitivity (96%) to 64-row multidetector arrays for detecting aneurysms greater than 4 mm diameter. However, for aneurysms < 4-mm multidetector arrays are significantly better with a sensitivity of 92% compared 75% for a single array [30]. Other series looking at small aneurysms < 3 mm report a sensitivity falling to 86–92% [31–33]. While sub-3-mm aneurysms have a lower rupture risk and are unlikely to be treated, a false negative still has implications for decisions on further surveillance imaging for the patient.

A weakness of CT angiography is detecting aneurysms near the skull base due to artifact from the bone. Bone subtraction CT is one technique to avoid this problem [34]. Other limitations include venous contamination with "kissing artifacts" of veins adjacent to arteries resembling aneurysms and the misrepresentation of infundibula as aneurysms where the apex vessel is too small to be resolved on CT imaging [35].

CT angiography can also be used as part of surveillance programs to monitor for aneurysm growth; however, there are no studies comparing its performance against a gold standard. In the absence of this comparison an in vitro phantom-based study was performed which showed poor ability of CT angiography to detect aneurysm growth with only a 58% detection rate for linear growth [36]. Despite this, CT angiography has been demonstrated to be effective in detecting aneurysm growth or bleb formation on aneurysm follow-up in the clinical setting [37]. The risk of causing cancer from a CT-based surveillance programs is relatively low and reaches 0.1% in men and 0.03% in woman [38] after 51 annual CT angiograms. Furthermore, the risk per exposure increases roughly by 0.0026% on average per CTA performed.

MRA

MRA is often preferred for aneurysm detection because it avoids ionizing radiation combined with its low cost and relatively quick acquisition. MRA may also include VWI techniques that facilitate the analysis of aneurysm wall enhancement [39]. Meta-analysis has shown that the sensitivity of time-of-flight (TOF) MRA for detecting aneurysms is 95%, which rises to 97% for contrast-enhanced (CE)-MRA [40]. The sensitivity of 3 T MRA was better (98 vs. 92%, $p = 0.054$) than lower field strengths for detecting aneurysms [40]. In a single-center series directly comparing 3 T-TOF with CE-MRA, the sensitivity of CE-MRA for aneurysm detection was considerably higher than TOF (0.95 vs. 0.86). Direct comparison of 64-row CTA and 3 T TOF MRA has shown a comparable sensitivity for aneurysm detection [41].

More recently, 7 T MRA is available for clinical use which has improved signal-to-noise ratio compared to 3 T. 7 T MRA is comparable to DSA for assessing UIA morphology [42] and reduces over-diagnosis of unruptured aneurysms in equivocal imaging compared to 3 T [43, 44] with greater interrater reliability and diagnostic certainty [44]. However, 7 T MRA is available in a limited number of centers and is not routinely used in screening UIAs.

Despite the high sensitivity of MRA for aneurysm detection, it shows worse performance for determining aneurysm morphology. The sensitivity for detecting irregularity of the aneurysm sac is only 60% compared to DSA [45]. This has implications for risk assessment given the links between sac irregularity and rupture described above. MRA for growth surveillance also needs to be used with some caution as a phantom model study has

shown that detection rates for aneurysm growth of only 54% [46] and clinically serial MRA measurements have up to 10% margin of error compared to 3D rotational angiography [47]. MRA is also unable to determine vessel/aneurysm calcification, which is an important technical factor, particularly when considering microsurgical clip reconstruction.

DSA

Digital subtraction angiography is an invasive catheter-based imaging modality which has good spatial and temporal resolution of luminal blood flow. It has long been considered the gold standard method for cerebrovascular imaging however its invasive nature carries risks such as stroke, radiation exposure, and iodine-based contrast complications. The rate of permanent stroke following DSA in large modern series is approximately 0.1–0.5% [48–51]. It is therefore used for assessment and treatment planning of known aneurysms rather than screening although it is possible for UIA to be incidentally diagnosed on DSA performed for another aneurysm given its higher sensitivity than CTA/MRA.

The next evolution from two-dimension DSA is 3D rotational angiography (3DRA). This involves a spin of the X-ray tube around a patient during catheter angiogram with machine-injected contrast. It allows 3D reconstruction for better visualization of the vascular anatomy and provides significant benefits over 2D DSA for detecting small aneurysms (< 2–3 mm) missed on 2D DSA [52, 53]. In addition to being the gold standard for IA size quantification and vessel visualization, DSA provides fluoroscopic imaging which is critical during endovascular IA treatment. Clinicians routinely use contrast-based DSA imaging to navigate the catheter, endovascular treatment, and to assess efficacy of the endovascular procedure.

Advanced Imaging Applications

Although conventional imaging like CTA and MRA are widely prevalent in clinical aneurysm detection and management, studies have shown that they can grossly underestimate the volume and size of saccular IAs as compared to gold standard catheter angiography [54, 55]. This could lead to subjectivity and misinformed rupture risk assessment of UIAs or treatment planning. Additionally, they offer limited spatial resolution and pathobiological insight [56]. To this end, recent advances in imaging modalities and techniques have led to new, more complex imaging that can offer additional information on the IA wall pathobiology.

Vessel Wall Imaging

VWI is a potential imaging biomarker for IA growth and rupture [57, 58]. Herein, a T1 weighted pre-contrast MRI is performed as a baseline scan, followed by a gadolinium (Gd)-based T1 weighted post-contrast MRI. IAs that demonstrate an uptake of the contrast (observed in the post-contrast MRI) are said to exhibiting aneurysm wall enhancement (AWE). Multiple cross-sectional as well as longitudinal studies have shown that IAs that have positive AWE are more likely to grow and be symptomatic [59–62].

Early qualitative studies have used subjective adjudication of AWE, generally described as circumferential or focal enhancement. The intensity of enhancement has also been adjudicated subjectively as weak versus strong [61, 63, 64]. This subjective assessment has high inter-user variability, especially in smaller IAs [65]. To better quantify AWE objectively, few first-order metrics using IA wall signal intensities on the post-contrast MRI normalized to intensities at different landmarks in the brain like the pituitary stalk or corpus callosum have been proposed [66]. Others have used the relative difference between pre- and post-contrast MRI [66, 67]. However, these first order metrics could not quantify the distribution of contrast across the aneurysm wall and only quantified the average enhancement. To address this, recent studies have focused on leveraging three-dimensional (3D) mapping of AWE and engineering features from these 3D maps. While some groups used histogram-based analysis of pre- and post-contrast MRI [68], others quantified the percentage of enhancing areas in the IA wall [69] (Fig. 1). Although, these semi-automated approaches could result in better visualization and robust quantification of AWE, the features obtained are limited.

Recently Veeturi et al. have demonstrated the potential utility of radiomics in the quantification and analysis of AWE [70]. Radiomics is a high-dimensional data characterization tool that quantifies the textural pattern of a region of interest which in our case would be the distribution of intensities on the aneurysm wall. The authors demonstrated that radiomics-based quantification of AWE outperforms conventional metrics such as the ratio obtained after normalization with the pituitary stalk (CR_{Stalk}) and the ratio obtained after normalization with the corpus callsoum (CC_{Ratio}). Quantification of AWE has progressed significantly in the past decade and future studies should address the validation of these methodologies in multi-center and longitudinal cohorts.

One of the key aspects of AWE is its potential correlation with histological changes in the aneurysm wall, suggestive of inflammation and aneurysm wall degradation [71]. Initial observations by Hasan et al. have suggested that macrophages may phagocytose super-magnetic particles like ferumoxytol, allowing the in vivo imaging of aneurysm wall inflammation [72]. However, due to the black box nature of

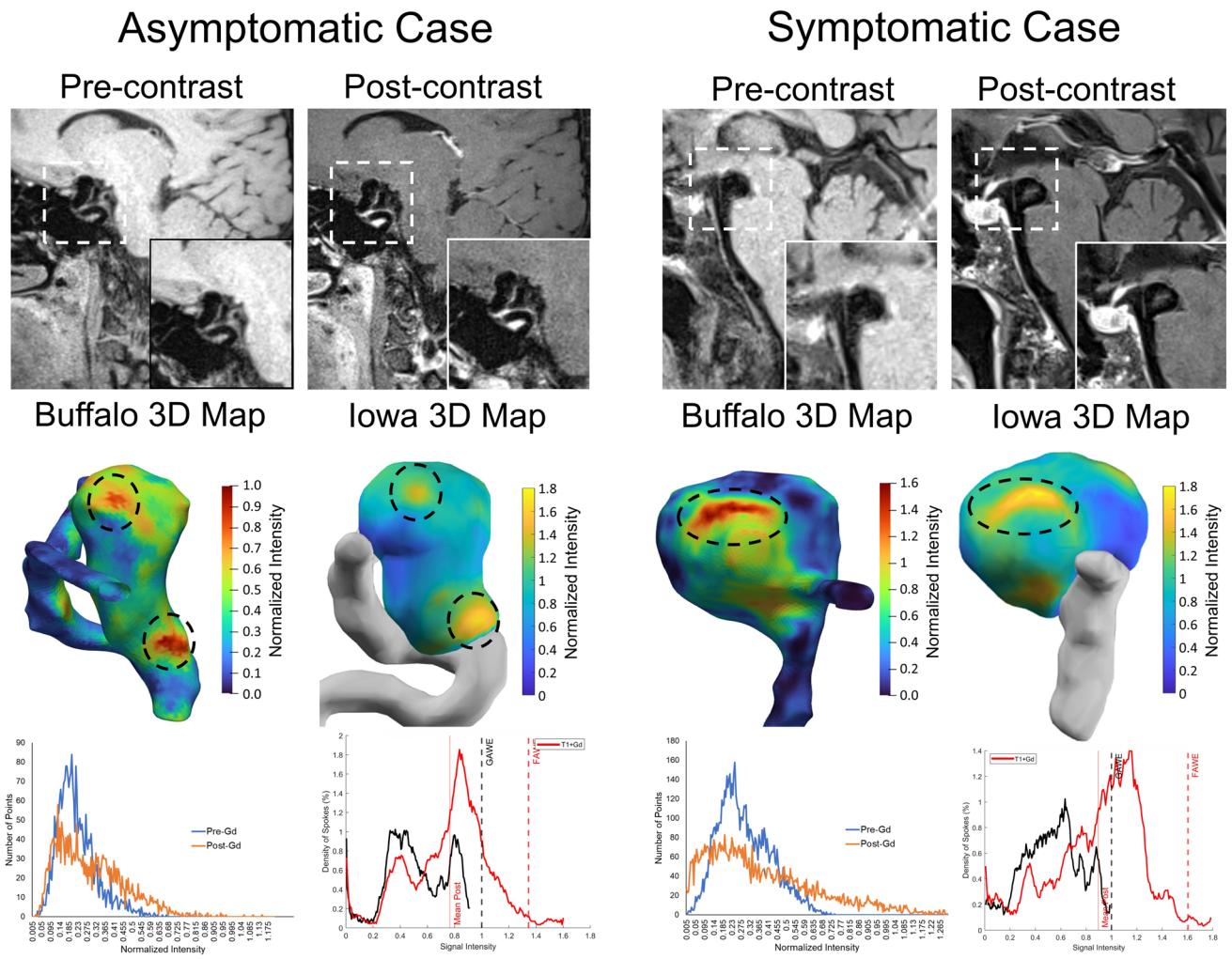

Fig. 1 Representative symptomatic and asymptomatic cases. The top row shows the pre-contrast and post-contrast MRI scans on the sagittal plane with the aneurysm enclosed in the white box. The second row shows the 3D mapping of intensity normalized to the corpus callosum using two different pipelines (from Buffalo and Iowa, respectively). We observe similar intensity distributions using both pipelines (encircled in the figure). The bottom row shows the histogram of normalized intensities using both mapping techniques. We observe higher distribution of high-intensity points on the symptomatic case due to aneurysm wall enhancement (AWE)

this contrast agent, further studies lacked interest paving the way for Gd-based contrast agents [73]. Although Gd had a shorter half-life (29 min) as compared to ferumoxytol (15 h), which reduces the window for post-contrast scan time, Gd is extensively used in clinical MRI studies [74]. Multiple histopathological studies have demonstrated a correlation between gadolinium enhancement and inflammation, neovascularization, and presence of vaso-vasorum [71, 75–77]. A few studies have also shown that partially thrombosed and IA with microbleeds can also exhibit focal AWE [63, 78, 79]. Future studies based on pooled large cohorts and better quantitative metrics of AWE can help unveil nuances in type of enhancement and underlying histopathology.

Over the years, multiple clinical risk assessment metrics have been developed to assess the risk of IA rupture like PHASES, UIATS, and ELAPSS [19, 22, 80]. In follow-up studies, these have been shown to correlate well with IA growth which is also an important indicator of impending IA rupture [81, 82]. Other studies have tried to use local IA hemodynamics and morphology to complement clinical information but have not gained traction [83, 84]. The major reason being that although these clinical metrics can be used as a back of the envelop evaluation of IA risk, they do not convey any pathobiological information. As AWE can be used as an indicator of local IA wall inflammation, this can be used to complement current clinical metrics. Indeed, past studies have demonstrated that AWE does not correlate well with existing clinical metrics such as PHASES and ELAPSS mostly because they are primarily based on the size of the IA [85]. Hence, objectively quantified AWE can be used as an

additional tool to complement current clinical management of IA risk assessment and treatment.

4D Flow and CFD

Aneurysm formation, growth, and rupture are a complex multi-faceted process. A potential key component in the process of aneurysm growth and rupture is the local hemodynamics inside the aneurysm sac [86]. Numerous tools have been developed in the past for hemodynamic assessment of IAs. Recently, phase contrast MRI (PC-MRI) has emerged as a non-invasive tool for hemodynamic assessment of IAs. PC-MRI relies on the quantification of blood causing a change in "phase" as compared to stationary non-flowing tissue. Phase refers to the alignment of the protons with respect to the MRI scanner's magnetic field. Generally, there are two images acquired, one with a phase encoding gradient and one without. The phase encoding gradient creates a difference in MRI signal intensity between stationary and moving fluids which is proportional to the velocity of the fluid. These two images are then subtracted from each other to yield a difference image that has just information about the velocity of the moving fluid. This was initially used on 2D slices across cross-sections to get planar velocity values and has now evolved into 3D temporally resolved flow information called 4D flow [87]. Hemodynamic metrics such as wall shear stress (WSS), oscillatory shear index (OSI), and relative residence time (RRT) derived from 4D flow have been used in the past for risk assessment of IAs [88, 89]. Hence, hemodynamics obtained from direct measurement of flow using 4D flow can give an additional modality of patient-specific information which can add to existing IA specific data.

4D flow outputs 3D flow information such as velocity of blood flowing through the arteries and in the IA. Velocity fields can then be processed to obtain relevant hemodynamic metrics such as WSS, OSI, and RRT. High values of WSS and positive WSS gradient have been hypothesized to play a key role in IA formation through loss of internal elastic lamina, media thinning, and bulge formation [90–92]. WSS has also been used for hemodynamics-based risk stratification of IAs although the true mechanism remains unknown [86, 93]. Pathobiological studies have shown that both abnormally high and low WSS are correlated with local inflammation of IA wall with high WSS having more inflammation [94]. Studies have also shown that lower WSS can give raise to slow recirculating flow in the aneurysm, leading to potential deposition of atherosclerotic plaques [95, 96]. Similarly, WSS divergence, which is a measure of the stretch being exerted on the IA wall, has also been shown to be associated with thicker looking walls [97]. OSI is another commonly used hemodynamic metric that measures the directional change of WSS in a cardiac cycle. OSI has been associated with higher wall permeability in porcine models which could explain why a combination of high OSI and low WSS is a favorable environment for IA formation and rupture [98, 99]. Apart from these, studies have also shown that non-traditional metrics such as RRT, pressure, transverse WSS, etc., can also be used for risk stratification of IAs as well as gaining pathobiological insights [84, 96, 100, 101].

4D flow is an extremely useful and accurate tool for hemodynamic characterization of IAs as it is based on the flow of the arteries. However, one of the major limitations is the resolution of information and potential imaging artifacts [102–104]. To this end, computational fluid dynamics (CFD) has also emerged as a potential tool where the Navier–Stokes equations are solved using different discretization schemes (finite volume solvers are most commonly used). A brief comparison of salient features of both is listed in Table 1. The most important difference is the lack of resolution in 4D flow and the lack of accuracy in CFD [105, 106]. Hence, studies have proposed using a combination of both, wherein 4D flow derived boundary conditions are used in CFD to compute high-resolution patient-specific hemodynamics [107].

4D flow is a clinically viable tool for assessment of intra-aneurysmal hemodynamics as it is a direct measurement of in vivo flow without additional processing. However, high spatial and temporal resolution scans warrant higher scan times which is not ideal [87]. To this end, recent studies have introduced new methodologies wherein scan time is ~ 10 min with 0.5 mm isotropic spatial resolution and a temporal resolution of 30 ms [108]. Furthermore, a recent study by Abderezai et al. introduced aFlow (which is based on 4D flow) to quantify wall movement in aneurysms [109]. The authors then used this algorithm to quantify differences

Table 1 Salient features and differences between 4D flow and CFD

4D flow	CFD
Direct imaging	In-silico computation
Based on velocity of blood	Based on generic inlet and outlet assumptions
Low spatial and temporal resolution	High spatial and temporal resolution
High accuracy to in vivo flow	Moderate to low accuracy based on assumptions
Acquisition time ~ 10 min	A few hours based on resolution
High uncertainties in hemodynamic metrics	High resolution hemodynamic metrics

in wall motion between stable and unstable aneurysms [110]. These advances in 4D flow show an increasing trend of translational research with reduced scan times and quantification of patient-specific features. Future studies should aim at using CFD and 4D flow in tandem for better assessment of patient-specific hemodynamics.

The comprehensive analysis of aneurysms with different imaging techniques that include VWI, CFDs, and finite element analysis allows a better analysis of the potential mechanisms of aneurysm formation, growth, and rupture. Raghuram et al. has shown with 7 T MRI that areas of focal high AWE in the sac and blebs of UIAs are associated with low wall tension, low wall shear stress, and low flow conditions [111]. Conversely, the neck had average AWE, high wall tension, high wall shear stress, and high flow conditions. The aneurysm dome and the aneurysm neck have different morpho-mechanical environments, with increased mechanical load at the neck. These findings, suggest that the neck of the aneurysm is exposed to higher flow conditions, which may lead to an inflammatory process within the wall, which lead to aneurysm growth and ultimately aneurysm rupture.

4D CTA

4D CTA is similar to 4D flow wherein temporal data of the IA is recorded for imaging blood flow or wall motion using the basic principles of CTA [112]. Herein, CTA images are acquired dynamically throughout the cardiac cycle with usually low scan time (estimates putting it between 30 s to a few minutes). However, one of the major differences between CTA and 4D-CTA is the amount of radiation dosage. Although the individual dosage of each CTA acquisition can be lower than conventional CTA, the cumulative dosage of a 4D CTA (which is the sum of all individual acquisitions) is substantially higher [113]. Reduction of dosage in individual acquisitions leads to more noise in the scan; however, image filtering techniques could help reduce dosage with low or no change to image quality [114].

4D CTA has been used in the evaluation of morphology of IAs. In a recent study, Dissaux et al. found that IA volume (among others) and volume variation had the least inter- and intra-user variability and can be obtained using a low cumulative 4D CTA dosage (0.6 mSv) [115]. 4D CTA can also be used in tandem with electrocardiogram (ECG) gating for clinical evaluation of IA morphology. A recent study by Yang et al. compared morphological metrics derived from ECG-gated 4D CTA against gold standard DSA [116]. They observed high correlation in determining the location ($k=1.0$), shape ($k=0.76$), diameter ($k=0.94$), and neck ($k=0.79$) of the IA. Notably, they observed that the dosage required for 4D CTA was lower than the DSA (0.32 vs. 0.84 mSv).

Recent studies have used 4D CTA for quantification of wall motion during the cardiac cycle [117, 118]. A study by Gu et al. demonstrated that there were significant differences in IA morphology (aspect ratio and size ratio) and pulsation points between ruptured and unruptured IAs computed through ECG gated 4D-CTA [119]. A similar study by Zhou et al. on a large cohort of 217 IAs showed that irregular pulsation of IA as well as IA morphology were independently associated with IA rupture [120]. Another study on a cohort of 117 IAs, the authors performed 4D CTA and observed that IAs with irregular pulsation had a 6-fold higher risk as compared to IAs without pulsation [121]. Indeed, quantification of wall motion through high-resolution 4D CTA could help in rupture risk stratification. Future studies could focus on augmenting traditional low-dosage 4D CTA with deep learning to increase spatiotemporal resolution which could help improve detection and rupture risk assessment of IAs [122].

AI Applications

Deep learning in management of IAs has gained a lot of traction over the past decade [123–127]. Deep learning (frequently termed as artificial intelligence or AI) is used for multiple applications; however, in the context of IAs, it is primarily used for detection, risk stratification, or treatment planning. Briefly, deep learning is a tool wherein a model such as 2D or 3D convolutional neural networks (CNN) are "trained" using a dataset of examples of the task to be performed which could be any of the above-mentioned applications. The model is then tested on an independent testing dataset to evaluate the performance through difference metrics specific to the task at hand.

For the detection of IAs, studies have used either a standalone CNN or used it to better assist a user. A recent meta-analysis on the application of deep learning for IA detection showed that IA detection using standalone deep learning techniques has a sensitivity of 91.2% and specificity of 83.5% (ROC-AUC = 0.936), whereas the deep-learning assisted user detection of IAs had a sensitivity of 90.3% and specificity of 92.1% (ROC-AUC = 0.91)[126]. Once an IA has been detected, accurate segmentation is paramount for assessment of morphology which is dependent on the underlying imaging modality. Deep learning–based segmentation approaches typically use either a U-Net architecture or some variation of it [128]. A commonly used metric to evaluate the accuracy of segmentation in deep learning is dice similarity coefficient (DSC) defined as

$$DSC = \frac{2 * |A \cap B|}{|A| + |B|}$$

where A and B are the ground truth segmentation and the deep learning segmentation output, respectively [129]. Studies using CTA as the base modality for segmentation

have demonstrated lower performance in IA morphology evaluation (DSC = 0.57–0.77) [130]. Similarly, a study by Ham et al. also demonstrated moderate DSC when using TOF-MRA as the imaging modality (DSC = 0.755) [131]. A recent study by Nishi et al. used 3D rotational angiography and demonstrated a high segmentation accuracy (mean DSC = 0.87, median DSC = 0.92) [132]. This is due to the higher resolution and better signal-to-noise ratio of the rotational angiography as compared to CTA and TOF-MRA [118]. A potential solution to mitigate this challenge is to use a combination of modalities. Indeed, recently Patel et al. demonstrated that training a deep learning model using a combination of DSA and CTA pairs results in better segmentation of CTA images [133]. Herein, they demonstrated a novel approach where a *DeepMedic* architecture was used to train a model which could segment a CTA scan at the resolution of a DSA. They also demonstrated that this approach leads to better identification of aneurysms and more accurate morphological assessment of IAs.

The segmented geometry is then used for risk stratification. A common approach is to derive morphological features such as size, size ratio, and aspect ratio, to train a simple logistic regression model or a machine learning model to identify high-risk IAs which could be defined through rupture status, IA growth, or symptomatic status. A recent study by Lin et al. demonstrated that in a cohort of 322 MCA aneurysms, machine learning models can be trained with an accuracy of 75% solely based on IA morphology and patient demographics [134]. To make this approach more clinical, studies have developed nomograms based on IA morphology and patient demographics that can readily be used in a clinical setting [135]. Another approach to rupture risk stratification is directly using a CNN on the input image as demonstrated in a study by Kim et al. [136]. Herein, the authors used six images proximal to the IA from different directions as input to predict the rupture status of an IA. They showed that the CNN had an accuracy of 77% on an independent test dataset. In addition to morphology assessment, deep learning can also be used as a tool for accelerating hemodynamic assessment of IAs. Hemodynamic evaluation of IAs is a complicated process and generally takes a few hours using CFD. In an effort to decrease computational cost, recent studies have started exploring physics informed neural networks (PINNS) as a potential tool to augment conventional CFD calculations [137]. A recent study by Sarabian et al. demonstrated the potential utility of PINNS wherein they used a combination of TOF-MRA and transcranial Doppler measurements from different locations in the brain to predict velocity and pressure maps in the major brain vessels [138]. Additionally, they also validated the outputs through 4D flow and observed an error of 0.2% in their best model.

Although deep learning has demonstrated an ability to perform similar to a clinician within reasonable error, its ability to handle bulk data warrants notice. Automated segmentation, morphological assessment, risk assessment, and treatment planning can all be done with the help of deep learning tools [125]. However, this has not gained traction as a viable clinical tool primarily due to its lack of interpretability black box nature [139]. Research groups have started to develop studies targeted toward "explainable AI" and using "attention maps"; however, demonstration of this in a clinical setting is still lacking [140]. The hope is that deep learning can be used as a tool to augment current clinical practice and potentially reduce time for IA workup, assessment, and treatment planning.

Conclusions

Imaging of IAs is continually advancing, encompassing applications such as detection, detailed characterization, and identification of biological processes occurring within the aneurysm wall. The deployment of high-resolution imaging techniques, more powerful scanners, sophisticated post-acquisition protocols, and AI technology enhances our ability to accurately characterize aneurysms. These advancements not only facilitate improved diagnosis and management but also drive the development of customized treatment strategies, ultimately enhancing patient outcomes.

Author Contribution Conceptualization: all authors; writing: SSV, SH; review and editing: EAS, VMT; final approval: all authors.

Funding This work is partially funded by the Brain Aneurysm Foundation.

Data Availability No datasets were generated or analysed during the current study.

Declarations

Competing Interests VMT: Financial interest/investor/stockoptions/ownership: Neurovascular Diagnostics, Inc., QAS.AI, Inc.;Consultant/advisory board: Canon Medical Systems USA; Researchgrants: Principal investigator, National Science Foundation Award No.1746694 and NIH NINDS award R43 NS115314-0; awardee of a Brain Aneurysm Foundation grant, a Center for Advanced Technology grant, and a Cummings Foundation grant

EAS: Consultant for Medtronic, Microvention, Cerenovus, iSchemaView, and Rapid Medical.

References

1. Vlak MH, Algra A, Brandenburg R, Rinkel GJ. Prevalence of unruptured intracranial aneurysms, with emphasis on sex, age,

comorbidity, country, and time period: a systematic review and meta-analysis. Lancet Neurol. 2011;10:626–36.
2. Kim JH, Kim JW, Song SW, Ahn SJ, Park M, Park SK, et al. Intracranial aneurysms are associated with Marfan syndrome: single cohort retrospective study in 118 patients using brain imaging. Stroke. 2021;52:331–4.
3. Sanchis IM, Shukoor S, Irazabal MV, Madsen CD, Chebib FT, Hogan MC, et al. Presymptomatic screening for intracranial aneurysms in patients with autosomal dominant polycystic kidney disease. Clin J Am Soc Nephrol. 2019;14:1151–60.
4. Kim JH, Lee KY, Ha SW, Suh SH. Prevalence of unruptured intracranial aneurysms: a single center experience using 3T brain MR angiography. Neurointervention. 2021;16:117–21.
5. Imaizumi Y, Mizutani T, Shimizu K, Sato Y, Taguchi J. Detection rates and sites of unruptured intracranial aneurysms according to sex and age: an analysis of MR angiography-based brain examinations of 4070 healthy Japanese adults. J Neurosurg. 2018;130:573–8.
6. Cras TY, Bos D, Ikram MA, Vergouwen MDI, Dippel DWJ, Voortman T, et al. Determinants of the presence and size of intracranial aneurysms in the general population: the Rotterdam Study. Stroke. 2020;51:2103–10.
7. Artico M, Spoletini M, Fumagalli L, Biagioni F, Ryskalin L, Fornai F, et al. Egas Moniz: 90 years (1927–2017) from cerebral angiography. Front Neuroanat. 2017;11:81.
8. Moniz E. L'Encéphalographie artérielle, son importance dans la localisation des tumeurs cérébrales, par Egas Moniz (de Lisbonne): Masson; 1927.
9. Dandy WE. Ventriculography following the injection of air into the cerebral ventricles. Ann Surg. 1918;68.
10. Sanchez S, Hickerson M, Patel RR, Ghazaleh D, Tarchand R, Paranjape GS, et al. Morphological Characteristics of Ruptured Brain Aneurysms: A Systematic Literature Review and Meta-Analysis. Stroke Vasc Interv Neurol. 2023;3.
11. Rajabzadeh-Oghaz H, Varble N, Shallwani H, Tutino VM, Mowla A, Shakir HJ, et al. Computer-assisted three-dimensional morphology evaluation of intracranial aneurysms. World Neurosurg. 2018;119:e541–50.
12. Paliwal N, Tutino VM, Shallwani H, Beecher JS, Damiano RJ, Shakir HJ, et al. Ostium ratio and neck ratio could predict the outcome of sidewall intracranial aneurysms treated with flow diverters. AJNR Am J Neuroradiol. 2019;40:288–94.
13. Damiano RJ, Tutino VM, Paliwal N, Patel TR, Waqas M, Levy EI, et al. Aneurysm characteristics, coil packing, and post-coiling hemodynamics affect long-term treatment outcome. J Neurointerv Surg. 2020;12:706–13.
14. Paliwal N, Jaiswal P, Tutino VM, Shallwani H, Davies JM, Siddiqui AH, et al. Outcome prediction of intracranial aneurysm treatment by flow diverters using machine learning. Neurosurg Focus. 2018;45:E7.
15. Morita A, Kirino T, Hashi K, Aoki N, Fukuhara S, Hashimoto N, et al. The natural course of unruptured cerebral aneurysms in a Japanese cohort. N Engl J Med. 2012;366:2474–82.
16. Wiebers DO, Whisnant JP, Huston J, Meissner I, Brown RD, Piepgras DG, et al. Unruptured intracranial aneurysms: natural history, clinical outcome, and risks of surgical and endovascular treatment. Lancet. 2003;362:103–10.
17. Juvela S, Poussa K, Lehto H, Porras M. Natural history of unruptured intracranial aneurysms: a long-term follow-up study. Stroke; a journal of cerebral circulation. 2013;44:2414–21.
18. Wiebers DO. Unruptured intracranial aneurysms: natural history, clinical outcome, and risks of surgical and endovascular treatment. The Lancet. 2003;362:103–10.
19. Greving JP, Wermer MJ, Brown RD Jr, Morita A, Juvela S, Yonekura M, et al. Development of the PHASES score for prediction of risk of rupture of intracranial aneurysms: a pooled analysis of six prospective cohort studies. The Lancet Neurology. 2014;13:59–66.
20. Murayama Y, Takao H, Ishibashi T, Saguchi T, Ebara M, Yuki I, et al. Risk analysis of unruptured intracranial aneurysms: prospective 10-year cohort study. Stroke. 2016;47:365–71.
21. Mocco J, Brown RD, Torner JC, Capuano AW, Fargen KM, Raghavan ML, et al. Aneurysm morphology and prediction of rupture: an international study of unruptured intracranial aneurysms analysis. Neurosurgery. 2018;82:491–6.
22. Backes D, Rinkel GJE, Greving JP, Velthuis BK, Murayama Y, Takao H, et al. ELAPSS score for prediction of risk of growth of unruptured intracranial aneurysms. Neurology. 2017;88:1600–6.
23. Etminan N, Brown RD, Beseoglu K, Juvela S, Raymond J, Morita A, et al. The unruptured intracranial aneurysm treatment score: a multidisciplinary consensus. Neurology. 2015;85:881–9.
24. Laukka D, Kivelev J, Rahi M, Vahlberg T, Paturi J, Rinne J, et al. Detection rates and trends of asymptomatic unruptured intracranial aneurysms from 2005 to 2019. Neurosurgery. 2023;94:297–306.
25. Friedman JA, Piepgras DG, Pichelmann MA, Hansen KK, Brown RD Jr, Wiebers DO. Small cerebral aneurysms presenting with symptoms other than rupture. Neurology. 2001;57:1212.
26. Mossa-Basha M, Zhu C, Yuan C, Saba L, Saloner DA, Edjlali M, et al. Survey of the American Society of Neuroradiology Membership on the use and value of intracranial vessel wall MRI. AJNR Am J Neuroradiol. 2022;43:951–7.
27. Hall S, Abouharb A, Anderson I, Bacon A, Bahl A, Brydon H, et al. A survey of the radiological follow-up of unruptured intracranial aneurysms in the United Kingdom. Br J Neurosurg. 2023;37:163–9.
28. Meijer FJA, Schuijf JD, de Vries J, Boogaarts HD, van der Woude WJ, Prokop M. Ultra-high-resolution subtraction CT angiography in the follow-up of treated intracranial aneurysms. Insights Imaging. 2019;10:2.
29. Hodgson KE, Larkin EA, Aznar MC, Vasquez Osorio E. Dual-energy computed tomography: Survey results on current uses and barriers to further implementation. Br J Radiol. 2021;94.
30. Menke J, Larsen J, Kallenberg K. Diagnosing cerebral aneurysms by computed tomographic angiography: meta-analysis. Ann Neurol. 2011;69:646–54.
31. Yang ZL, Ni QQ, Schoepf UJ, De Cecco CN, Lin H, Duguay TM, et al. Small intracranial aneurysms: diagnostic accuracy of CT angiography. Radiology. 2017;285:941–52.
32. Lu L, Zhang LJ, Poon CS, Wu SY, Zhou CS, Luo S, et al. Digital subtraction CT angiography for detection of intracranial aneurysms: comparison with three-dimensional digital subtraction angiography. Radiology. 2012;262:605–12.
33. Li Q, Lv F, Yao G, Li Y, Xie P. 64-section multidetector CT angiography for evaluation of intracranial aneurysms: comparison with 3D rotational angiography. Acta Radiol. 2014;55:840–6.
34. Cheng B, Cai W, Sun C, Kang Y, Gong J. 3D bone subtraction CT angiography for the evaluation of intracranial aneurysms: a comparison study with 2D bone subtraction CT angiography and conventional non-subtracted CT angiography. Acta Radiol. 2015;56:1127–34.
35. Takhtani D. CT neuroangiography: a glance at the common pitfalls and their prevention. AJR Am J Roentgenol. 2005;185:772–83.
36. Al Kasab S, Nakagawa D, Zanaty M, Bathla G, Policeni B, Soni N, et al. In vitro accuracy and inter-observer reliability of CT angiography in detecting intracranial aneurysm enlargement. J Neurointerv Surg. 2019;11:1015–8.
37. Villablanca JP, Duckwiler GR, Jahan R, Tateshima S, Martin NA, Frazee J, et al. Natural history of asymptomatic unruptured cerebral aneurysms evaluated at CT angiography: growth and

rupture incidence and correlation with epidemiologic risk factors. Radiology. 2013;269:258–65.
38. Malhotra A, Wu X, Chugh A, Mustafa A, Matouk CC, Gandhi D, et al. Risk of radiation-induced cancer from computed tomography angiography use in imaging surveillance for unruptured cerebral aneurysms. Stroke. 2019;50:76–82.
39. Sanchez S, Gudino-Vega A, Guijarro-Falcon K, Miller JM, Noboa LE, Samaniego EA. MR imaging of the cerebral aneurysmal wall for assessment of rupture risk. Neuroimaging Clin N Am. 2024;34:225–40.
40. Sailer AM, Wagemans BA, Nelemans PJ, de Graaf R, van Zwam WH. Diagnosing intracranial aneurysms with MR angiography: systematic review and meta-analysis. Stroke. 2014;45:119–26.
41. Hiratsuka Y, Miki H, Kiriyama I, Kikuchi K, Takahashi S, Matsubara I, et al. Diagnosis of unruptured intracranial aneurysms: 3T MR angiography versus 64-channel multi-detector row CT angiography. Magn Reson Med Sci. 2008;7:169–78.
42. Wrede KH, Matsushige T, Goericke SL, Chen B, Umutlu L, Quick HH, et al. Non-enhanced magnetic resonance imaging of unruptured intracranial aneurysms at 7 Tesla: comparison with digital subtraction angiography. Eur Radiol. 2017;27:354–64.
43. Radojewski P, Slotboom J, Joseph A, Wiest R, Mordasini P. Clinical implementation of 7T MRI for the identification of incidental intracranial aneurysms versus anatomic variants. AJNR Am J Neuroradiol. 2021;42:2172–4.
44. Radojewski P, Dobrocky T, Branca M, Almiri W, Correia M, Raabe A, et al. Diagnosis of Small Unruptured Intracranial Aneurysms : Comparison of 7 T versus 3 T MRI. Clin Neuroradiol. 2023.
45. Kwak Y, Son W, Kim YS, Park J, Kang DH. Discrepancy between MRA and DSA in identifying the shape of small intracranial aneurysms. J Neurosurg. 2020;134:1887–93.
46. Nakagawa D, Nagahama Y, Policeni BA, Raghavan ML, Dillard SI, Schumacher AL, et al. Accuracy of detecting enlargement of aneurysms using different MRI modalities and measurement protocols. J Neurosurg. 2018;130:559–65.
47. Raghuram A, Patel R, Varon A, Sabotin R, Sanchez S, Derdeyn CP, et al. Volumetric surveillance of brain aneurysms: pitfalls of MRA. Interv Neuroradiol. 2023;29:532–9.
48. Tafelmeier S, Kesseler E, Iancu AM, Nikoubashman O, Wiesmann M. Spectrum of complications and complication rates after diagnostic catheter angiography in neuroradiology. Clin Neuroradiol. 2023;33:763–8.
49. Fifi JT, Meyers PM, Lavine SD, Cox V, Silverberg L, Mangla S, et al. Complications of modern diagnostic cerebral angiography in an academic medical center. J Vasc Interv Radiol. 2009;20:442–7.
50. Willinsky RA, Taylor SM, TerBrugge K, Farb RI, Tomlinson G, Montanera W. Neurologic complications of cerebral angiography: prospective analysis of 2,899 procedures and review of the literature. Radiology. 2003;227:522–8.
51. Kaufmann TJ, Huston J, Mandrekar JN, Schleck CD, Thielen KR, Kallmes DF. Complications of diagnostic cerebral angiography: evaluation of 19,826 consecutive patients. Radiology. 2007;243:812–9.
52. van Rooij WJ, Sprengers ME, de Gast AN, Peluso JP, Sluzewski M. 3D rotational angiography: the new gold standard in the detection of additional intracranial aneurysms. AJNR Am J Neuroradiol. 2008;29:976–9.
53. Shi WY, Li YD, Li MH, Gu BX, Chen SW, Wang W, et al. 3D rotational angiography with volume rendering: the utility in the detection of intracranial aneurysms. Neurol India. 2010;58:908–13.
54. Raghuram A, Patel R, Varon A, Sabotin R, Sanchez S, Derdeyn CP, et al. Volumetric surveillance of brain aneurysms: Pitfalls of MRA. Interv Neuroradiol. 2022;29:532–9.
55. Munarriz PM, Bárcena E, Alén JF, Castaño-Leon AM, Paredes I, Moreno-Gómez LM, et al. Reliability and accuracy assessment of morphometric measurements obtained with software for three-dimensional reconstruction of brain aneurysms relative to cerebral angiography measures. Interv Neuroradiol. 2020;27:191–9.
56. Diab R, Chang D, Zhu C, Levitt MR, Aksakal M, Zhao HL, et al. Advanced cross-sectional imaging of cerebral aneurysms. Br J Radiol. 2023;96:20220686.
57. Texakalidis P, Hilditch CA, Lehman V, Lanzino G, Pereira VM, Brinjikji W. Vessel wall imaging of intracranial aneurysms: systematic review and meta-analysis. World Neurosurg. 2018;117(453–8): e1.
58. Samaniego EA, Roa JA, Hasan D. Vessel wall imaging in intracranial aneurysms. J Neurointerv Surg. 2019;11:1105–12.
59. Matsushige T, Shimonaga K, Ishii D, Sakamoto S, Hosogai M, Hashimoto Y, et al. Vessel wall imaging of evolving unruptured intracranial aneurysms. Stroke. 2019;50:1891–4.
60. Omodaka S, Endo H, Niizuma K, Fujimura M, Inoue T, Endo T, et al. Circumferential wall enhancement in evolving intracranial aneurysms on magnetic resonance vessel wall imaging. J Neurosurg. 2018;131:1262–8.
61. Edjlali M, Gentric JC, Regent-Rodriguez C, Trystram D, Hassen WB, Lion S, et al. Does aneurysmal wall enhancement on vessel wall MRI help to distinguish stable from unstable intracranial aneurysms? Stroke. 2014;45:3704–6.
62. Raghuram A, Sanchez S, Wendt L, Cochran S, Ishii D, Osorno C, et al. 3D aneurysm wall enhancement is associated with symptomatic presentation. J Neurointerv Surg. 2022;neurintsurg-2022-019125.
63. Matsushige T, Shimonaga K, Mizoue T, Hosogai M, Hashimoto Y, Kaneko M, et al. Focal aneurysm wall enhancement on magnetic resonance imaging indicates intraluminal thrombus and the rupture point. World Neurosurg. 2019;127:e578–84.
64. Edjlali M, Guedon A, Ben Hassen W, Boulouis G, Benzakoun J, Rodriguez-Regent C, et al. Circumferential thick enhancement at vessel wall MRI has high specificity for intracranial aneurysm instability. Radiology. 2018;289:181–7.
65. Veeturi SS, Pinter N, Baig A, Monteiro A, Rai HH, Patel T, et al. 3D Mapping of Vessel Wall Enhancement could Assist in Robust Risk Stratification of Intracranial Aneurysms. In: 2022 IEEE Western New York Image and Signal Processing Workshop (WNYISPW). 2022. p. 1–5.
66. Omodaka S, Endo H, Niizuma K, Fujimura M, Inoue T, Sato K, et al. Quantitative assessment of circumferential enhancement along the wall of cerebral aneurysms using MR imaging. AJNR Am J Neuroradiol. 2016;37:1262–6.
67. Wang GX, Wen L, Lei S, Ran Q, Yin JB, Gong ZL, et al. Wall enhancement ratio and partial wall enhancement on MRI associated with the rupture of intracranial aneurysms. J Neurointerv Surg. 2018;10:566–70.
68. Raghuram A, Varon A, Roa JA, Ishii D, Lu Y, Raghavan ML, et al. Semiautomated 3D mapping of aneurysmal wall enhancement with 7T-MRI. Sci Rep. 2021;11:18344.
69. Veeturi SS, Pinter NK, Monteiro A, Baig AA, Rai HH, Waqas M, et al. An Image-Based Workflow for Objective Vessel Wall Enhancement Quantification in Intracranial Aneurysms. Diagn (Basel). 2021;11.
70. Veeturi SS, Raghuram A, Miller J, Pinter NK, Sanchez S, Baig AA, et al. Radiomics Features in Contrast-Enhanced and Non-enhanced Magnetic Resonance Imaging Images Are Associated With High Intracranial Aneurysmal Risk. Stroke Vasc Interv Neurol. 2023;3.
71. Samaniego EA. Brain Aneurysm Biology: What Can We Learn From Imaging? Stroke Vasc Interv Neurol. 2022;2.
72. Hasan D, Chalouhi N, Jabbour P, Dumont AS, Kung DK, Magnotta VA, et al. Early change in ferumoxytol-enhanced magnetic resonance imaging signal suggests unstable human cerebral aneurysm: a pilot study. Stroke. 2012;43:3258–65.

73. Rubin R. Black Box Warning for Anemia Drug. JAMA. 2015;313:1704.
74. Vergouwen MDI, Backes D, van der Schaaf IC, Hendrikse J, Kleinloog R, Algra A, et al. Gadolinium enhancement of the aneurysm wall in unruptured intracranial aneurysms is associated with an increased risk of aneurysm instability: a follow-up study. AJNR Am J Neuroradiol. 2019;40:1112–6.
75. Larsen N, von der Brelie C, Trick D, Riedel CH, Lindner T, Madjidyar J, et al. Vessel wall enhancement in unruptured intracranial aneurysms: an indicator for higher risk of rupture? High-resolution MR imaging and correlated histologic findings. AJNR Am J Neuroradiol. 2018;39:1617–21.
76. Zhong W, Su W, Li T, Tan X, Chen C, Wang Q, et al. Aneurysm wall enhancement in unruptured intracranial aneurysms: a histopathological evaluation. J Am Heart Assoc. 2021;10:e018633.
77. Dinia L, Vert C, Gramegna LL, Arikan F, Hernández D, Coscojuela P, et al. Wall enhancement as a biomarker of intracranial aneurysm instability: a histo-radiological study. Acta Neurochir. 2023;165:2783–91.
78. Shimonaga K, Matsushige T, Ishii D, Sakamoto S, Hosogai M, Kawasumi T, et al. Clinicopathological insights from vessel wall imaging of unruptured intracranial aneurysms. Stroke. 2018;49:2516–9.
79. Roa JA, Zanaty M, Piscopo AJ, Morris TW, Sabotin R, Ishii D, et al. Contrast enhancement of brain aneurysms on high-resolution vessel wall imaging [HR-VWI] correlates with the presence of microbleeds. Cardiol Cardiovasc Med. 2021;05.
80. Etminan N, Brown RD, Beseoglu K, Juvela S, Raymond J, Morita A, et al. The unruptured intracranial aneurysm treatment score. Neurology. 2015;85:881.
81. Backes D, Vergouwen MD, Tiel Groenestege AT, Bor AS, Velthuis BK, Greving JP, et al. PHASES score for prediction of intracranial aneurysm growth. Stroke. 2015;46:1221–6.
82. Brinjikji W, Pereira VM, Khumtong R, Kostensky A, Tymianski M, Krings T, et al. PHASES and ELAPSS scores are associated with aneurysm growth: a study of 431 unruptured intracranial aneurysms. World Neurosurg. 2018;114:e425–32.
83. Rajabzadeh-Oghaz H, Waqas M, Veeturi SS, Vakharia K, Tso MK, Snyder KV, et al. A data-driven model to identify high-risk aneurysms and guide management decisions: the Rupture Resemblance Score. J Neurosurg. 2020;135:9–16.
84. Detmer FJ, Chung BJ, Mut F, Slawski M, Hamzei-Sichani F, Putman C, et al. Development and internal validation of an aneurysm rupture probability model based on patient characteristics and aneurysm location, morphology, and hemodynamics. Int J Comput Assist Radiol Surg. 2018;13:1767–79.
85. Roa JA, Sabotin RP, Varon A, Raghuram A, Patel D, Morris TW, et al. Performance of Aneurysm Wall Enhancement Compared with Clinical Predictive Scales: PHASES, ELAPSS, and UIATS. World Neurosurg. 2021;147:e538–51.
86. Meng H, Tutino VM, Xiang J, Siddiqui A. High WSS or low WSS? Complex interactions of hemodynamics with intracranial aneurysm initiation, growth, and rupture: toward a unifying hypothesis. AJNR Am J Neuroradiol. 2014;35:1254–62.
87. Markl M, Frydrychowicz A, Kozerke S, Hope M, Wieben O. 4D flow MRI. J Magn Reson Imaging. 2012;36:1015–36.
88. Perera R, Isoda H, Ishiguro K, Mizuno T, Takehara Y, Terada M, et al. Assessing the risk of intracranial aneurysm rupture using morphological and hemodynamic biomarkers evaluated from magnetic resonance fluid dynamics and computational fluid dynamics. Magn Reson Med Sci. 2020;19:333–44.
89. Youn SW, Lee J. From 2D to 4D phase-contrast MRI in the neurovascular system: will it be a quantum jump or a fancy decoration? J Magn Reson Imaging. 2022;55:347–72.
90. Metaxa E, Tremmel M, Natarajan SK, Xiang J, Paluch RA, Mandelbaum M, et al. Characterization of critical hemodynamics contributing to aneurysmal remodeling at the basilar terminus in a rabbit model. Stroke. 2010;41:1774–82.
91. Kolega J, Gao L, Mandelbaum M, Mocco J, Siddiqui AH, Natarajan SK, et al. Cellular and molecular responses of the basilar terminus to hemodynamics during intracranial aneurysm initiation in a rabbit model. J Vasc Res. 2011;48:429–42.
92. Meng H, Wang Z, Hoi Y, Gao L, Metaxa E, Swartz DD, et al. Complex hemodynamics at the apex of an arterial bifurcation induces vascular remodeling resembling cerebral aneurysm initiation. Stroke. 2007;38:1924–31.
93. Detmer FJ, Chung BJ, Jimenez C, Hamzei-Sichani F, Kallmes D, Putman C, et al. Associations of hemodynamics, morphology, and patient characteristics with aneurysm rupture stratified by aneurysm location. Neuroradiology. 2019;61:275–84.
94. Cebral J, Ollikainen E, Chung BJ, Mut F, Sippola V, Jahromi BR, et al. Flow conditions in the intracranial aneurysm lumen are associated with inflammation and degenerative changes of the aneurysm wall. AJNR Am J Neuroradiol. 2017;38:119–26.
95. Cebral JR, Detmer F, Chung BJ, Choque-Velasquez J, Rezai B, Lehto H, et al. Local hemodynamic conditions associated with focal changes in the intracranial aneurysm wall. AJNR Am J Neuroradiol. 2019;40:510–6.
96. Veeturi SS, Patel TR, Baig AA, Chien A, Monteiro A, Waqas M, et al. Hemodynamic Analysis Shows High Wall Shear Stress Is Associated with Intraoperatively Observed Thin Wall Regions of Intracranial Aneurysms. J Cardiovasc Dev Dis. 2022;9.
97. Kim JH, Han H, Moon YJ, Suh S, Kwon TH, Kim JH, et al. Hemodynamic Features of Microsurgically Identified, Thin-Walled Regions of Unruptured Middle Cerebral Artery Aneurysms Characterized Using Computational Fluid Dynamics. Neurosurg. 2020;86:851-9.
98. Himburg HA, Grzybowski DM, Hazel AL, LaMack JA, Li X-M, Friedman MH. Spatial comparison between wall shear stress measures and porcine arterial endothelial permeability. Am J Physiol Heart Circ Physiol. 2004;286:H1916–22.
99. Xiang J, Natarajan SK, Tremmel M, Ma D, Mocco J, Hopkins LN, et al. Hemodynamic-morphologic discriminants for intracranial aneurysm rupture. Stroke. 2011;42:144–52.
100. Cebral JR, Mut F, Weir J, Putman C. Quantitative characterization of the hemodynamic environment in ruptured and unruptured brain aneurysms. AJNR Am J Neuroradiol. 2011;32:145–51.
101. Cebral JR, Mut F, Weir J, Putman CM. Association of hemodynamic characteristics and cerebral aneurysm rupture. AJNR Am J Neuroradiol. 2011;32:264–70.
102. Puiseux T, Sewonu A, Meyrignac O, Rousseau H, Nicoud F, Mendez S, et al. Reconciling PC-MRI and CFD: an in-vitro study. NMR Biomed. 2019;32:e4063.
103. Castle-Kirszbaum M, Maingard J, Lim RP, Barras CD, Kok HK, Chandra RV, et al. Four-dimensional magnetic resonance imaging assessment of intracranial aneurysms: a state-of-the-art review. Neurosurgery. 2020;87:453–65.
104. Karmonik C, Diaz O, Grossman R, Klucznik R. In-vivo quantification of wall motion in cerebral aneurysms from 2D cine phase contrast magnetic resonance images. Rofo. 2010;182:140–50.
105. van Ooij P, Potters WV, Guedon A, Schneiders JJ, Marquering HA, Majoie CB, et al. Wall shear stress estimated with phase contrast MRI in an in vitro and in vivo intracranial aneurysm. J Magn Reson Imaging. 2013;38:876–84.
106. van Ooij P, Schneiders JJ, Marquering HA, Majoie CB, van Bavel E, Nederveen AJ. 3D cine phase-contrast MRI at 3T in intracranial aneurysms compared with patient-specific computational fluid dynamics. AJNR Am J Neuroradiol. 2013;34:1785–91.
107. Rutkowski DR, Roldan-Alzate A, Johnson KM. Enhancement of cerebrovascular 4D flow MRI velocity fields using machine learning and computational fluid dynamics simulation data. Sci Rep. 2021;11:10240.

108. Gottwald LM, Toger J, Markenroth Bloch K, Peper ES, Coolen BF, Strijkers GJ, et al. High spatiotemporal resolution 4D flow MRI of intracranial aneurysms at 7T in 10 minutes. AJNR Am J Neuroradiol. 2020;41:1201–8.
109. Abderezaei J, Martinez J, Terem I, Fabris G, Pionteck A, Yang Y, et al. Amplified flow imaging (aFlow): a novel MRI-based tool to unravel the coupled dynamics between the human brain and cerebrovasculature. IEEE Trans Med Imaging. 2020;39:4113–23.
110. Pionteck A, Abderezaei J, Fillingham P, Chuang Y-C, Sakai Y, Belani P, et al. Intracranial aneurysm wall displacement depicted by amplified Flow predicts growth. J Neurointerv Surg. 2024;jnis-2023-021227.
111. Raghuram A, Galloy A, Nino M, Sanchez S, Hasan D, Raghavan S, et al. Comprehensive morphomechanical analysis of brain aneurysms. Acta neurochir. 2023;165:461–70.
112. Kortman HG, Smit EJ, Oei MT, Manniesing R, Prokop M, Meijer FJ. 4D-CTA in neurovascular disease: a review. AJNR Am J Neuroradiol. 2015;36:1026–33.
113. Yang CY, Chen YF, Lee CW, Huang A, Shen Y, Wei C, et al. Multiphase CT angiography versus single-phase CT angiography: comparison of image quality and radiation dose. AJNR Am J Neuroradiol. 2008;29:1288–95.
114. Mendrik AM, Vonken EJ, van Ginneken B, de Jong HW, Riordan A, van Seeters T, et al. TIPS bilateral noise reduction in 4D CT perfusion scans produces high-quality cerebral blood flow maps. Phys Med Biol. 2011;56:3857–72.
115. Dissaux B, Ognard J, Cheddad El Aouni M, Nonent M, Haioun K, Magro E, et al. Volume variation may be a relevant metric in the study of aneurysm pulsatility: a study using ECG-gated 4D-CTA (PULSAN). J Neurointerv Surg. 2020;12:632–6.
116. Yang L, Gao X, Gao C, Xu S, Cao S. Dynamic evaluation of unruptured intracranial aneurysms by 4D-CT angiography: comparison with digital subtraction angiography (DSA) and surgical findings. BMC Med Imaging. 2023;23:161.
117. Stam LB, Aquarius R, de Jong GA, Slump CH, Meijer FJA, Boogaarts HD. A review on imaging techniques and quantitative measurements for dynamic imaging of cerebral aneurysm pulsations. Sci Rep. 2021;11:2175.
118. Maupu C, Lebas H, Boulaftali Y. Imaging modalities for intracranial aneurysm: more than meets the eye. Front Cardiovasc Med. 2022;9:793072.
119. Gu Y, Zhang Y, Luo M, Zhang H, Liu X, Miao C. Risk Factors for asymptomatic intracranial small aneurysm rupture determined by electrocardiographic-gated 4D computed tomographic (CT) angiography. Med Sci Monit. 2020;26:e921835.
120. Zhou J, Guo Q, Chen Y, Lin B, Ding S, Zhao H, et al. Irregular pulsation of intracranial aneurysm detected by four-dimensional CT angiography and associated with small aneurysm rupture: a single-center prospective analysis. Front Neurol. 2022;13:809286.
121. Zhang J, Li X, Zhao B, Zhang J, Sun B, Wang L, et al. Irregular pulsation of intracranial unruptured aneurysm detected by four-dimensional CT angiography is associated with increased estimated rupture risk and conventional risk factors. J Neurointerv Surg. 2021;13:854–9.
122. Wang J, Sun J, Xu J, Lu S, Wang H, Huang C, et al. Detection of intracranial aneurysms using multiphase CT angiography with a deep learning model. Acad Radiol. 2023;30:2477–86.
123. Bizjak Ž, Špiclin Ž. A Systematic Review of Deep-Learning Methods for Intracranial Aneurysm Detection in CT Angiography. Biomedicines. 2023;11:2921.
124. Li X, Zeng L, Lu X, Chen K, Yu M, Wang B, et al. A Review of Artificial Intelligence in the Rupture Risk Assessment of Intracranial Aneurysms: Applications and Challenges. Brain Sciences. 2023;13:1056.
125. Mensah E, Pringle C, Roberts G, Gurusinghe N, Golash A, Alalade AF. Deep learning in the management of intracranial aneurysms and cerebrovascular diseases: a review of the current literature. World Neurosurg. 2022;161:39–45.
126. Din M, Agarwal S, Grzeda M, Wood DA, Modat M, Booth TC. Detection of cerebral aneurysms using artificial intelligence: a systematic review and meta-analysis. J Neurointerv Surg. 2023;15:262–71.
127. Patel TR, Paliwal N, Jaiswal P, Waqas M, Mokin M, Siddiqui AH, et al. Multi-resolution CNN for brain vessel segmentation from cerebrovascular images of intracranial aneurysm: a comparison of U-Net and DeepMedic. In: Medical Imaging 2020: Computer-Aided Diagnosis: SPIE. 2020. p. 677–85.
128. Ronneberger O, Fischer P, Brox T. U-net: Convolutional networks for biomedical image segmentation. Medical image computing and computer-assisted intervention–MICCAI 2015: 18th international conference, Munich, Germany, October 5-9, 2015, proceedings, part III 18: Springer; 2015. p. 234-41.
129. Zou KH, Warfield SK, Bharatha A, Tempany CM, Kaus MR, Haker SJ, et al. Statistical validation of image segmentation quality based on a spatial overlap index. Acad Radiol. 2004;11:178–89.
130. Bo ZH, Qiao H, Tian C, Guo Y, Li W, Liang T, et al. Toward human intervention-free clinical diagnosis of intracranial aneurysm via deep neural network. Patterns. 2021;2:100197.
131. Ham S, Seo J, Yun J, Bae YJ, Kim T, Sunwoo L, et al. Automated detection of intracranial aneurysms using skeleton-based 3D patches, semantic segmentation, and auxiliary classification for overcoming data imbalance in brain TOF-MRA. Sci Rep. 2023;13:12018.
132. Nishi H, Cancelliere NM, Rustici A, Charbonnier G, Chan V, Spears J, et al. Deep learning-based cerebral aneurysm segmentation and morphological analysis with three-dimensional rotational angiography. J Neurointerv Surg. 2024;16:197–203.
133. Patel TR, Patel A, Veeturi SS, Shah M, Waqas M, Monteiro A, et al. Evaluating a 3D deep learning pipeline for cerebral vessel and intracranial aneurysm segmentation from computed tomography angiography–digital subtraction angiography image pairs. Neurosurg focus. 2023;54:E13.
134. Lin M, Xia N, Lin R, Xu L, Chen Y, Zhou J, et al. Machine learning prediction model for the rupture status of middle cerebral artery aneurysm in patients with hypertension: a Chinese multicenter study. Quant Imaging Med Surg. 2023;13:4867–78.
135. Liu J, Chen Y, Zhu D, Li Q, Chen Z, Zhou J, et al. A nomogram to predict rupture risk of middle cerebral artery aneurysm. Neurol Sci. 2021;42:5289–96.
136. Kim HC, Rhim JK, Ahn JH, Park JJ, Moon JU, Hong EP, et al. Machine learning application for rupture risk assessment in small-sized intracranial aneurysm. J Clin Med. 2019;8:683.
137. Moser P, Fenz W, Thumfart S, Ganitzer I, Giretzlehner M. Modeling of 3D blood flows with physics-informed neural networks: comparison of network architectures. Fluids. 2023;8:46.
138. Sarabian M, Babaee H, Laksari K. Physics-informed neural networks for brain hemodynamic predictions using medical imaging. IEEE Trans Med Imaging. 2022;41:2285–303.
139. Shi Z, Hu B, Schoepf UJ, Savage RH, Dargis DM, Pan CW, et al. Artificial intelligence in the management of intracranial aneurysms: current status and future perspectives. AJNR Am J Neuroradiol. 2020;41:373–9.
140. An J, Joe I. Attention map-guided visual explanations for deep neural networks. Appl Sci. 2022;12:3846.